

Finite-Temperature Properties of Multiferroic BiFeO₃

Igor A. Kornev,^{1,2} S. Lisenkov,¹ R. Haumont,³ B. Dkhil,⁴ and L. Bellaiche¹

¹*Physics Department, University of Arkansas, Fayetteville, Arkansas 72701, USA*

²*Mads Clausen Institute for Product Innovation, University of Southern Denmark, Alsion 2, DK-6400 Sønderborg, Denmark*

³*Laboratoire de Physico-Chimie de l'Etat Solide (CNRS), ICMMO, Université Paris XI, 91405 Orsay, France*

⁴*Laboratoire Structures, Propriétés et Modélisation des Solides, Ecole Centrale Paris, CNRS-UMR8580, Grande Voie des Vignes, 92295 Châtenay-Malabry Cedex, France*

(Received 5 July 2007; published 30 November 2007)

An effective Hamiltonian scheme is developed to study finite-temperature properties of multiferroic BiFeO₃. This approach reproduces very well (i) the symmetry of the ground state, (ii) the Néel and Curie temperatures, and (iii) the intrinsic magnetoelectric coefficients (that are very weak). This scheme also predicts (a) an overlooked phase above $T_C \approx 1100$ K that is associated with antiferrodistortive motions, as consistent with our additional x-ray diffractions, (b) improperlike dielectric features above T_C , and (c) that the ferroelectric transition is of first order with no group-subgroup relation between the paraelectric and polar phases.

DOI: 10.1103/PhysRevLett.99.227602

PACS numbers: 77.80.Bh, 75.50.Ee, 75.80.+q

Multiferroics form a class of materials that can simultaneously possess ferroelectricity and magnetic ordering [1]. They can therefore exhibit a magnetoelectric (ME) coupling that allows electrical properties to be tuned by a magnetic field or, conversely, magnetic properties to be varied by an electric field. These systems are experiencing a huge regain in interest (see, e.g., Ref. [2], and references therein). As a result, some controversial and/or puzzling effects have been recently reported in BiFeO₃ bulk—which is one of the most studied multiferroics, and has a T_N Néel temperature of ≈ 625 – 643 K [3,4] and another transition temperature around 1083–1103 K [4,5] at which the material transforms from a ferroelectric rhombohedral state to another phase. Examples of such effects are the symmetry of this latter high-temperature phase: is it paraelectric cubic [6], ferroelectric orthorhombic [7], or even something else that has been missed? Other intriguing features are the character of the phase transition around 1100 K (that is, said to be not soft-mode driven in Ref. [6]), and the magnetic-induced change of the dielectric constant that varies by several orders of magnitude for temperatures below versus above 175 K [8]—which raises questions about the value of the intrinsic ME coefficients or, equivalently, the importance of defects on the ME coupling in BiFeO₃ samples. First-principles techniques can lead to a better understanding of multiferroics (see, e.g., Refs. [9–11]), but not the point to address the aforementioned issues since these techniques are essentially restricted to the study

of zero-temperature properties and cannot currently compute ME coefficients. Ideally, one desires an atomisticlike scheme with the capability of accurately predicting properties of multiferroics at finite temperature, including their ME couplings.

The purpose of this Letter is to demonstrate that it is possible to develop such an “ideal” approach and to apply it to BiFeO₃ bulk. The use of this scheme, and additional x-ray measurements we further conducted, provide answers to all the aforementioned issues and also yield overlooked phenomena.

Our numerical scheme is based on the generalization of the effective Hamiltonian of Ref. [12] to include magnetic degrees of freedom, in addition to ferroelectric (FE) and antiferrodistortive (AFD) motions. The total energy, E_{tot} , is written as a sum of two main terms, $E_{\text{FE-AFD}}(\{\mathbf{u}_i\}, \{\eta_H\}, \{\eta_I\}, \{\omega_i\})$ and $E_{\text{MAG-C}}(\{\mathbf{m}_i\}, \{\mathbf{u}_i\}, \{\eta_H\}, \{\eta_I\}, \{\omega_i\})$, where $E_{\text{FE-AFD}}$ is the energy provided in Ref. [12], while $E_{\text{MAG-C}}$ is an additional term gathering magnetic degrees of freedom and their couplings. \mathbf{m}_i is the magnetic dipole moment centered on the Fe site i . \mathbf{u}_i is the (Fe-centered) local soft mode in unit cell i , which is directly proportional to the electrical dipole centered on that site; $\{\eta_H\}$ and $\{\eta_I\}$ are the homogeneous and inhomogeneous strain tensors [13], respectively; $\{\omega_i\}$ is a (Fe-centered) vector characterizing the direction and magnitude of the AFD motions in unit cell i .

For $E_{\text{MAG-C}}$, we propose the following expression:

$$E_{\text{MAG-C}}(\{\mathbf{m}_i\}, \{\mathbf{u}_i\}, \{\eta_H\}, \{\eta_I\}, \{\omega_i\}) = \sum_i \sum_{j \neq i} D_{ij} \mathbf{m}_i \cdot \mathbf{m}_j + \sum_i u_i^2 \sum_{j \neq i} E_{ij} \mathbf{m}_i \cdot \mathbf{m}_j + \sum_i [\eta_1(i) + \eta_2(i) + \eta_3(i)] \sum_{j \neq i} F_{ij} \mathbf{m}_i \cdot \mathbf{m}_j + \sum_i \omega_i^2 \sum_{j \neq i} G_{ij} \mathbf{m}_i \cdot \mathbf{m}_j, \quad (1)$$

where the sums over i run over all the Fe sites while the sums over j run over the first, second, and third nearest neighbors of the Fe site i . $\eta_l(i)$ is the l th component, in Voigt notation, of the total strain at the site i , with the x , y , and z axes being along the pseudocubic [100], [010], and [001] directions, respectively. The first term of Eq. (1) represents the exchange

interactions associated with local magnetic moments, while the last three terms characterize how the local soft-mode, strain, and AFD degrees of freedom modify these exchange interactions, respectively—with the D_{ij} , E_{ij} , F_{ij} , and G_{ij} coefficients quantifying such interactions and modifications. The parameters entering the analytical expression of E_{tot} are determined by performing LDA + U and LSDA + U calculations [14] (with no spin-orbit corrections) on paramagnetic, ferromagnetic, and antiferromagnetic BiFeO₃ supercells, using the PWSCF code [15] and adopting the value of 3.8 eV for U —that arises from the application of the proposed scheme of Ref. [16] to BiFeO₃.

E_{tot} is then used in Monte Carlo (MC) simulations to compute finite-temperature properties of BiFeO₃. We typically use $14 \times 14 \times 14$ supercells and up to 4×10^6 MC sweeps. The local magnetic moments $\{\mathbf{m}_i\}$ are assumed to have a fixed magnitude of $4\mu_B$, as consistent with first-principles computations [10]. Relevant outputs of the MC procedure are the $\langle \mathbf{u} \rangle$ supercell average of the $\{\mathbf{u}_i\}$, the $\langle \mathbf{m} \rangle$ supercell average of the $\{\mathbf{m}_i\}$, the $\langle \mathbf{m} \rangle_G$ vector defined as $\langle \mathbf{m} \rangle_G = \frac{1}{N} \sum_i \mathbf{m}_i (-1)^{n_x(i)+n_y(i)+n_z(i)}$, and the $\langle \omega \rangle_R$ vector for which $\langle \omega \rangle_R = \frac{1}{N} \sum_i \omega_i (-1)^{n_x(i)+n_y(i)+n_z(i)}$ where the last two sums run over the Fe sites and where $n_x(i)$, $n_y(i)$, and $n_z(i)$ are integers locating the cell i (the Fe site i is centered at $[n_x(i)\mathbf{x} + n_y(i)\mathbf{y} + n_z(i)\mathbf{z}]a$, where a is the 5-atom lattice constant and where \mathbf{x} , \mathbf{y} , and \mathbf{z} are unit vectors along the Cartesian axes). Nonvanishing $\langle \mathbf{u} \rangle$ and $\langle \mathbf{m} \rangle$ indicate ferroelectricity and ferromagnetism, respectively. Nonzero $\langle \mathbf{m} \rangle_G$ and $\langle \omega \rangle_R$ characterize G -type antiferromagnetism and AFD motions associated with the R point of the cubic first Brillouin zone, respectively.

Using this approach yields a Curie temperature, T_C , of 1105 ± 5 K which is rather close to the experimental value of 1083–1103 K [4,5]. On the other hand, the simulations overestimate the experimental value of $T_N \approx 625$ –643 K [3,4] by around 200 K. The accuracy can be further improved via a renormalization of the parameters of Eq. (1). This is confirmed by Figs. 1(a)–1(c) that display predictions arising from the use of the proposed scheme with the D_{ij} , E_{ij} , F_{ij} , and G_{ij} parameters having been reduced by 25% [17].

More precisely, Fig. 1(a) shows the Cartesian coordinates ($\langle u_1 \rangle$, $\langle u_2 \rangle$, and $\langle u_3 \rangle$) of $\langle \mathbf{u} \rangle$, Fig. 1(b) displays $\langle \omega \rangle_R$ (with $\langle \omega_1 \rangle_R$, $\langle \omega_2 \rangle_R$, and $\langle \omega_3 \rangle_R$ denoting the Cartesian coordinates of $\langle \omega \rangle_R$), and Fig. 1(c) reports the magnitudes of $\langle \mathbf{m} \rangle_G$ and $\langle \mathbf{m} \rangle$. Figures 1(a)–1(c) indicate that our approach predicts a $R3c$ ground state that exhibits (i) a polarization pointing along the [111] direction (since $\langle u_1 \rangle = \langle u_2 \rangle = \langle u_3 \rangle \neq 0$ at low temperatures), (ii) a tilting of the oxygen octahedra about the [111] axis (since $\langle \omega_1 \rangle_R = \langle \omega_2 \rangle_R = \langle \omega_3 \rangle_R \neq 0$ at low temperatures), and (iii) a G -type antiferromagnetism (with the magnitude of $\langle \mathbf{m} \rangle_G$ adopting its maximum value of $4\mu_B$ for $T \rightarrow 0$ K). Such predictions are consistent with both first-principles calculations [10] and experiments (see Ref. [6], and refer-

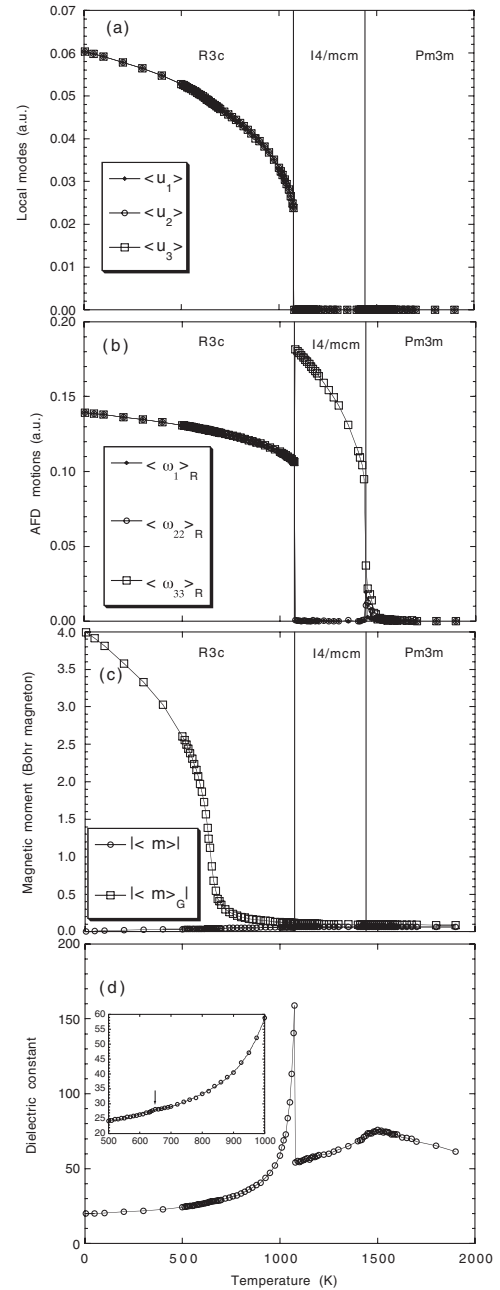


FIG. 1. Supercell average $\langle \mathbf{u} \rangle$ of the local mode vectors (a), AFD-related $\langle \omega \rangle_R$ quantity (b), magnetic moments (c), and dielectric constant (d), as a function of temperature in BiFeO₃ and as predicted by the presently proposed method with the parameters of Eq. (1) having been reduced by 25% with respect to their values computed within the LSDA + U technique—in which U is equal to 3.8 eV. The displayed dielectric constant is computed as one-third of the trace of the dielectric tensor. The inset of Fig. 1(d) emphasizes the kink of the dielectric constant around the Néel temperature.

ences therein) [18]. Other agreements with measurements [6] are that increasing the temperature from 0 K first leads to a transition (at $T_N \approx 635 \pm 5$ K, see inflexion point of $\langle \mathbf{m} \rangle_G$ in Fig. 1(c)) from a $R3c$ antiferromagnetic state to a $R3c$ paramagnetic state and then, at higher temperature (at

$T_C \approx 1075 \pm 5$ K), to the disappearance of ferroelectricity via a first-order transition—as indicated by the jump in $\langle \mathbf{u} \rangle$ seen in Fig. 1(a). Interestingly, Fig. 1(b) also offers a striking result: for temperatures just above T_C , BiFeO₃ is neither in a cubic paraelectric $Pm\bar{3}m$ state (as commonly thought [6]) nor in a ferroelectric orthorhombic phase (as recently proposed [7]) but rather exhibits a tetragonal $I4/mcm$ state that is associated with AFD motions [see the nonzero value of $\langle \omega_3 \rangle_R$ above ≈ 1080 K in Fig. 1(b)]. Such an overlooked phase is predicted to exist up to ≈ 1440 K, before transforming to $Pm\bar{3}m$. Moreover, Fig. 1(d) reveals that the dielectric constant, ϵ , slightly modifies its temperature behavior around T_N , and, in particular, exhibits a small kink around the Néel temperature. Such a kink has also been predicted in another multiferroic, that is, BiMnO₃ [20], and may be consistent with the phonon anomalies observed around T_N in Ref. [6]. Another interesting feature of Fig. 1(d) is that ϵ deviates from a Curie-Weiss law [21] in the tetragonal $I4/mcm$ phase: ϵ decreases (rather than increases) as the temperature is lowered from 1440 to 1075 K. Such dielectric feature is typical of improper ferroelectrics [22], as consistent with Ref. [8], and the ferroelectric transition is also of first order with no group-subgroup relation between $I4/mcm$ and $R3c$ —as consistent with the fact that the ferroelectric transition is said to be not soft-mode driven in Ref. [6].

To investigate intrinsic ME effects at room temperature, we apply a magnetic field \mathbf{B} and compute the induced change in electrical polarization and dielectric constant. Figure 2(a) reveals that the polarization adopts a quadratic behavior with the magnetic field, namely, $P = P_0 + \alpha B + \beta B^2$ with $P_0 \approx 0.64$ C/m², $\alpha = +3.0 \pm 0.9 \times 10^{-7}$ C/T · m², and $\beta = -3.38 \pm 0.03 \times 10^{-8}$ C/T² · m². P_0 compares rather well with the recently measured 300 K polarization of ≈ 0.50 – 0.60 C/m² [2].

Our predicted linear ME coefficient is very weak and remarkably close to the experimental one of $+4.1 \times 10^{-7}$ C/T · m² [23]. Similarly, the magnitude of the simulated β quadratic coefficient is of the same order than the measured ones ranging between 1.6×10^{-8} and 6.0×10^{-8} C/T² · m² that can be extracted from Ref. [24]. Moreover, Fig. 2(b) shows that the dielectric constant linearly increases with the magnetic field (as consistent with the magnetic-induced decrease of the polarization shown in Fig. 2(a)), i.e. $\epsilon = \epsilon_0 + \gamma B$ —with $\epsilon_0 \approx 22$ and $\gamma = 0.00052 \pm 0.00002$ per Tesla, which leads to $\frac{(\epsilon - \epsilon_0)}{(\epsilon_0 B)} \approx 2.4 \times 10^{-5}$ T⁻¹. This linear dependency has been observed in Ref. [8], and our predicted ϵ_0 and $\frac{(\epsilon - \epsilon_0)}{(\epsilon_0 B)}$ agree very well with those measured below 175 K [8]—namely, ϵ_0 of the order of 25–40 and $\frac{(\epsilon - \epsilon_0)}{(\epsilon_0 B)}$ ranging between 6.7×10^{-6} and 4.96×10^{-5} T⁻¹ when the temperature varies between 10 and 150 K. Such agreements confirm the assumption of Ref. [8]: the large ME effect [e.g., $\frac{(\epsilon - \epsilon_0)}{(\epsilon_0 B)} > 10^{-3}$ T⁻¹] and large dielectric constants (e.g., $\epsilon > 1000$),

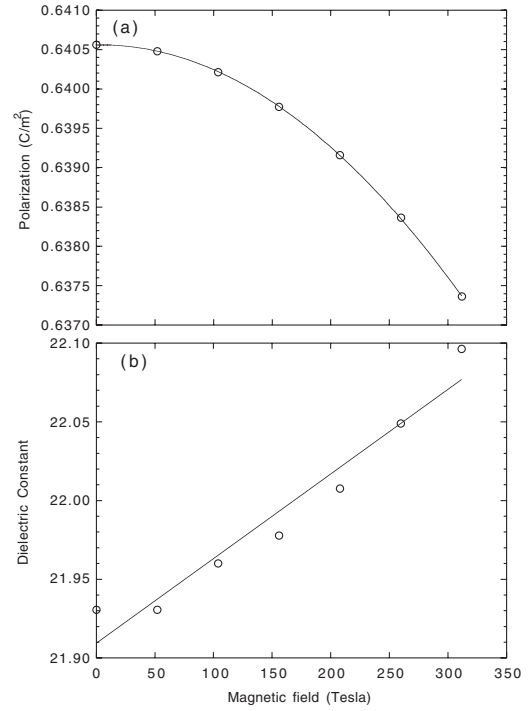


FIG. 2. Room-temperature polarization (a) and dielectric constant (b) of BiFeO₃, as a function of magnetic field and as predicted by the presently proposed method with the parameters of Eq. (1) having been reduced by 25% with respect to their values computed within the LSDA + U technique—in which U is equal to 3.8 eV. The displayed dielectric constant is computed as one-third of the trace of the dielectric tensor. The solid lines in (a) and (b) display quadratic and linear fits, respectively.

observed in BiFeO₃ for temperatures above 175 K are, in fact, due to extrinsic effects, such as Maxwell-Wagner phenomena occurring at the dielectric-electrode interfaces or at the grain boundaries in ceramics [25].

In parallel with our simulations, we have undertaken a x-ray analysis on a BiFeO₃ powder. The diffraction pattern from $2\Theta = 5^\circ$ to 120° with a step of 0.04° were collected with a Philips X-celerator Bragg-Brentano diffractometer equipped with a Copper source ($\lambda = 1.54056$ Å), from room temperature to 1400 K by steps of 10 K—by using a furnace with an accuracy of around 2 K. The room-temperature phase is found to be $R3c$ and no trace of any parasitic phase is evidenced. Above 1200 K, a decomposition into Bi₂Fe₄O₉ is observed (which may be related to the possible metal-insulator transition suggested in Ref. [7]) and the melting point is reached at 1240 K. This prevents us from checking our predictions of a $Pm\bar{3}m$ state above 1440 K indicated in Figs. 1 (our simulations concern BiFeO₃ in its solid perovskite state). Interestingly, for temperatures ranging between $T_C = 1100$ and 1200 K, the diffraction pattern exhibits multiple strong Bragg peaks but also additional weaker peaks, as shown in Fig. 3.

This pattern characterizes a noncubic state, as consistent with recent findings [7] while in contrast with what has

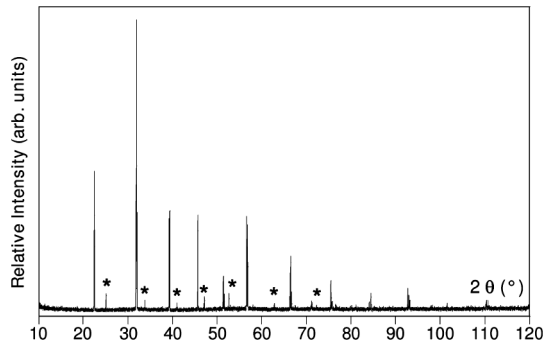


FIG. 3. The experimental x-ray spectra at 1110 K. The star symbols indicate the weaker, but important, peaks.

been previously reported [6]. Several heating-cooling processes demonstrate that this high-temperature phase is stable and reversible. In order to determine its symmetry, a Rietveld analysis at 1110 K was carried out with the XND software [26]. We first tested pure ferroelectric phases, that are $P4mm$, $Bmm2$, $R3m$, Cm , and Pm . Among all these phases, the best refinement is obtained with the orthorhombic $Bmm2$ space group, as consistent with Ref. [7], that reproduces rather well the strong Bragg peaks. However, the additional weaker peaks cannot be fitted by any ferroelectric state, including $Bmm2$. We then considered several other phases associated with antiferrodistortive motions with and without ferroelectric displacements—e.g., $R3c$, $R3c$, $Imma$, $Pnma$, Pc , Cc , $C2/m$, $I4cm$, $I4/mcm$, etc.—and even mixing of phases—e.g., $R3c + I4/mcm$. The best agreement factors and matching between the observed and calculated profiles are obtained with the monoclinic $C2/m$ model, which allows one to reconstruct both the strong and weak reflections. Interestingly, such a phase cannot be ferroelectric but rather is allowed to exhibit antiferrodistortive motions [27], as consistent with our predictions of a $I4/mcm$ phase shown in Fig. 1. Consistency between our measurements and predictions is further confirmed when knowing that the experimental lattice parameters of the $C2/m$ phase at $T = 1110$ K are $a = 5.6140(1)$ Å, $b = 7.9716(2)$ Å, and $c = 5.6461(1)$ Å with the monoclinic angle being extremely close to 90° , namely, $90.012(4)^\circ$. The $C2/m$ phase can thus be seen as pseudotetragonal. Note that the fact that our simulations miss the rather weak monoclinic distortions in favor of a pure tetragonal state may be due to higher-order terms neglected in the expression of the total energy or to an electronic rearrangement above T_C —since our model does not incorporate electronic degrees of freedom. It may also be caused by unavoidable defects in the samples, especially grain boundaries present in the powder, which calls for measurements on high-quality single crystals. In any case, our predictions and measurements both indicate an overlooked high-temperature phase that is neither cubic nor ferroelectric, but rather is associated with AFD motions.

This work is supported by ONR Grants No. N00014-04-1-0413 and No. N00014-01-1-0365 (CPD), by NSF Grants No. DMR-0404335 and No. DMR-0080054 (C-SPIN), and by DOE Grant No. DE-FG02-05ER46188. We thank S. Kamba and J. Iniguez for useful discussions.

-
- [1] G. A. Smolenskii and I. E. Chupis, *Sov. Phys. Usp.* **25**, 475 (1982).
 - [2] J. Wang *et al.*, *Science* **299**, 1719 (2003).
 - [3] P. Fischer *et al.*, *J. Phys. C* **13**, 1931 (1980).
 - [4] S. V. Kiselev *et al.*, *Sov. Phys. Dokl.* **7**, 742 (1963); G. A. Smolenskii *et al.*, *Sov. Phys. Solid State* **2**, 2651 (1961).
 - [5] J. R. Teague, R. Gerson, and W. J. James, *Solid State Commun.* **8**, 1073 (1970).
 - [6] R. Haumont *et al.*, *Phys. Rev. B* **73**, 132101 (2006).
 - [7] R. Palai, R. S. Katiyar, and J. F. Scott, arXiv:cond-mat/0705.2883v1.
 - [8] S. Kamba *et al.*, *Phys. Rev. B* **75**, 024403 (2007).
 - [9] N. A. Hill, *J. Phys. Chem. B* **104**, 6694 (2000).
 - [10] J. B. Neaton *et al.*, *Phys. Rev. B* **71**, 014113 (2005).
 - [11] P. Ravindran *et al.*, *Phys. Rev. B* **74**, 224412 (2006).
 - [12] I. Kornev *et al.*, *Phys. Rev. Lett.* **97**, 157601 (2006).
 - [13] W. Zhong, D. Vanderbilt, and K. M. Rabe, *Phys. Rev. Lett.* **73**, 1861 (1994).
 - [14] V. I. Anisimov, F. Aryasetiawan, and A. I. Lichtenstein, *J. Phys. Condens. Matter* **9**, 767 (1997).
 - [15] S. Baroni *et al.*, www.pwscf.org.
 - [16] M. Cococcioni and S. de Gironcoli, *Phys. Rev. B* **71**, 035105 (2005).
 - [17] The need for the renormalization of the magnetic-related parameters to obtain a very high accuracy may arise from the fact that the U parameter of the LSDA + U method [14] is not precisely known, while the coefficients of Eq. (1) are rather sensitive to it. For instance, a slight decrease of U from 3.8 to 3.5 eV already results in a reduction of 20% for some of these coefficients.
 - [18] BiFeO₃ is, in fact, observed to be nearly G -type antiferromagnetic, since experiments also report a cycloidal spiral arrangement of the magnetic moments with a length of 620 Å [19]. Such spiral structure is not found in our current simulations because it requires the use of rather large supercells or additional interactions with respect to those indicated in Eq. (1).
 - [19] I. Sosnowska *et al.*, *Physica (Amsterdam)* **180B**, 117 (1992).
 - [20] C. G. Zhong, J. H. Fang, and Q. Jiang, *J. Phys. Condens. Matter* **16**, 9059 (2004).
 - [21] C. Kittel, *Introduction to Solid State Physics* (Wiley, New York, 1996), 7th ed.
 - [22] B. A. Strukov and A. P. Levanyuk, *Ferroelectric Phenomena in Crystals* (Springer, Geidelberg, 1998), Chap. 4.
 - [23] J.-P. Rivera and H. Schmid, *Ferroelectrics* **204**, 23 (1997).
 - [24] V. A. Murashov *et al.*, *Ferroelectrics* **162**, 11 (1994).
 - [25] G. Catalan, *Appl. Phys. Lett.* **88**, 102902 (2006).
 - [26] J. F. Béjar and P. Lelann, *J. Appl. Crystallogr.* **24**, 1 (1991).
 - [27] H. T. Stokes *et al.*, *Acta Crystallogr. Sect. B* **58**, 934 (2002).